Liquid Crystals

Magnetic Properties of All-Organic Liquid Crystals Containing a Chiral Five-Membered Cyclic Nitroxide Unit within the Rigid Core

Naohiko Ikuma, Rui Tamura, Satoshi Shimono, Naoyuki Kawame, Osamu Tamada, Naoko Sakai, Jun Yamauchi, and Yukio Yamamoto*

The orientation of liquid crystals (LCs) can generally be controlled by magnetic and electric fields owing to their molecular magnetic and dielectric anisotropies, respectively. The threshold of the magnetic fields necessary to align liquid-crystalline substances decreases with increasing magnetic susceptibility anisotropy ($|\Delta\chi|$) of the mesogens and the decreasing viscosity of the material.[1] As the orientation of a diamagnetic calamitic organic LC by external magnetic fields is ascribed to the small diamagnetic susceptibility anisotropy ($0 < |\Delta\chi_{dia}| < 60 \times 10^{-6}$ emu mol^{-1}) of the mesogen which arises from the constituent aromatic rings,[2] relatively strong magnetic fields (> 1 T) are necessary for the orientation of this type of LC. Therefore, it is quite reasonable to take advantage of a paramagnetic susceptibility anisotropy ($\Delta\chi_{para}$) for the orientation of LCs by weak magnetic fields, because χ_{para} is usually one or two orders of magnitude larger than χ_{dia}. For this reason, a number of metallomesogens with permanent spins that originate from their transition-metal centers have been prepared.[1,3] Particularly, calamitic lanthanide-containing metallomesogens have a large paramagnetic anisotropy, but the intrinsic high viscosity brought about by the ligand-coordinated metal-complex structure frequently renders their orientation by weak magnetic fields difficult.[3]

In contrast, a calamitic organic LC with a stable nitroxyl (NO) group as a spin source can benefit from a small paramagnetic susceptibility anisotropy and a low viscosity by means of an appropriate molecular design; for example, 1) a cyclic nitroxide framework is incorporated into the rigid core of the mesogen to maximize the paramagnetic anisotropy, and 2) the side chains are extended from the two quaternary carbon atoms adjacent to the nitroxyl group to reduce the viscosity. Consequently, its orientation may be controlled by weak magnetic fields.

To test the above assumption, it is essential to find a prototype of the calamitic mesogen that exhibits an extremely stable paramagnetic liquid-crystalline phase. Furthermore, to obtain a series of mesogens showing the nematic and chiral-nematic (cholesteric) phases, and/or the smectic and chiral-smectic phases,[4] the prototypic molecular structure should be chiral. However, very few LCs containing the organic spin center have been prepared mainly because the geometry and bulkiness of the radical-stabilizing substituents are detrimental to the stability of liquid-crystalline phases. Their molecular structures were limited to those containing a nitroxyl group within the alkyl side chain, away from the rigid core and hence allowed the free rotation of the nitroxyl moiety inside the molecule, leading to a decrease in the paramagnetic anisotropy of the whole molecule.[5] Unfortunately, all attempts to prepare monomeric or polymeric mesogens by using the organic spin as part of the rigid core have been unsuccessful.[5,6]

With this in mind, we focused on the chiral 3,4-dihydro-2,5-dimethyl-2*H*-pyrrole 1-oxide (**1**) from which a variety of chiral derivatives can be prepared in the form of racemates or nonracemates (Scheme 1).[7] First we synthesized the C_2-symmetric *trans*-2,5-bis(alkoxyphenyl) derivatives **2a**–**e** with various alkyl side chains, but they were not liquid-crystalline—this was most likely a result of their compact molecular packing in the crystalline state as judged from the crystal structures of (±)-**2a** and (2*S*,5*S*)-**2a** (Figure 1).[8] We then modified the molecular structure to decrease the molecular symmetry and strengthen the core-to-core interactions in the liquid-crystalline state. Consequently, the C_1-symmetric *trans*-2-alkoxyphenyl-5-[4-(4-alkoxybenzenecarbonyloxy)phenyl] derivatives **3**, which have disordered alkyl side chains in the crystalline state (Figure 2), successfully exhibited enantiotropic liquid-crystalline phases over wide temperature ranges (see Table 1 and Supporting Information); the racemic samples of **3a**–**d** showed a Schlieren texture typical for a nematic phase by hot-stage polarizing microscopy (Figure 3a), whereas the corresponding nonracemic samples (94–97% *ee*) exhibited an oily-streak texture characteristic

[*] N. Ikuma, Prof. R. Tamura
Graduate School of Global Environmental Studies and
Graduate School of Human and Environmental Studies
Kyoto University, Kyoto 606-8501 (Japan)
Fax: (+81) 75-753-7915
E-mail: tamura@fischer.jinkan.kyoto-u.ac.jp
S. Shimono, N. Kawame, Prof. O. Tamada, N. Sakai,
Prof. Y. Yamamoto
Graduate School of Human and Environmental Studies
Kyoto University, Kyoto 606-8501 (Japan)
Prof. J. Yamauchi
Graduate School of Science, Kyoto University
Kyoto 606-8501 (Japan)

Supporting information for this article is available on the WWW under http://www.angewandte.org or from the author.

 DOI: 10.1002/ange.200460007

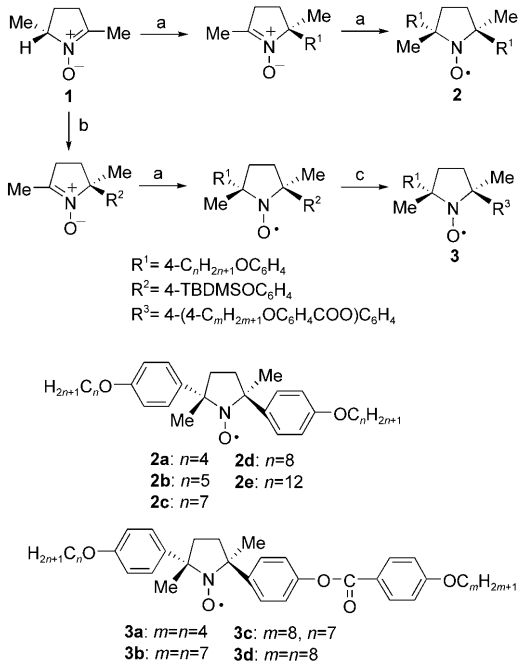

Scheme 1. Preparation of chiral nitroxides **2** and **3**. Reagents and conditions: a) 1. R^1MgBr, THF −78 °C; 2. $Cu(OAc)_2$, O_2; b) 1. R^2MgBr, −78 °C; 2. $Cu(OAc)_2$, O_2; c) TBAF, Et_3N. $C_mH_{2m+1}OC_6H_4COCl$, THF, 0 °C. TBAF = tetra-*n*-butylammonium fluoride

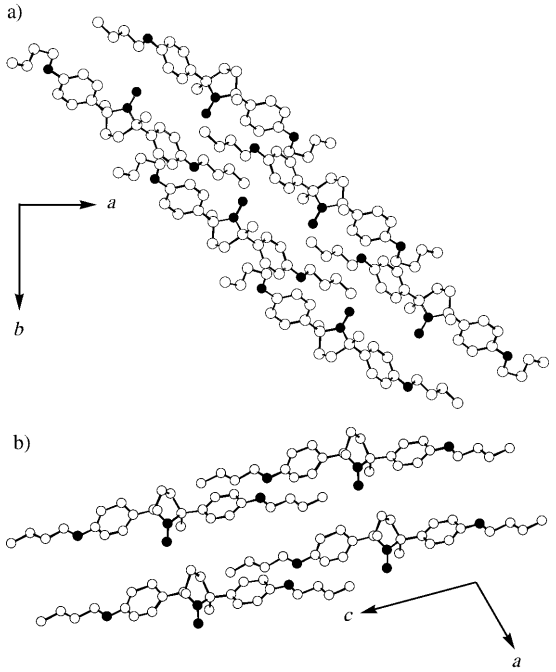

Figure 1. Crystal structures of a) (±)-**2a** and b) (2*S*,5*S*)-**2a**. The carbon, nitrogen, and oxygen atoms are represented by open, grid, and closed circles, respectively. Hydrogen atoms are omitted for clarity.

of a cholesteric phase (Figure 3b).[4] These liquid-crystalline phases are extremely thermally stable; for example, after allowing (±)-**3c** to stand at 73 °C for 24 h, there was no decrease in the purity of the material, and the racemic and nonracemic samples of **3a–d** did not decompose after several heating and cooling cycles between the individual melting and clearing points.

More interesting are the bulk magnetic properties of **3**. The magnetic susceptibilities of the racemic and nonracemic samples of **3a–d** were measured in a quartz tube (3.5 ϕ × 40 mm) on a SQUID susceptometer at a field of 0.5 T in the temperature range 2–380 K. During the first heating process starting from the crystalline phase, (±)-**3c** and (±)-**3d**

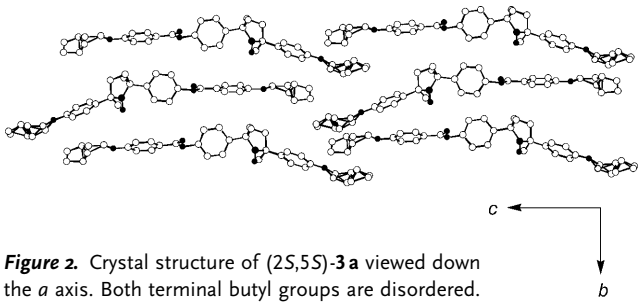

Figure 2. Crystal structure of (2*S*,5*S*)-**3a** viewed down the *a* axis. Both terminal butyl groups are disordered. The carbon, nitrogen, and oxygen atoms are represented by open, grid, and closed circles, respectively. Hydrogen atoms are omitted for clarity.

Table 1: Optical, magnetic, and thermal data of **3a–d**.

Compound	*ee* [%][a]	$[\alpha]_D^{26}$[b]	ESR[b] *g*	ESR[b] a_N [mT]	*C* [$emu^{-1}\,K\,mol^{-1}$][c]	θ [K][d]	Phase transition [°C][e]
(±)-**3a**	–	–	2.0068	1.34	0.37[f]	−0.04[f]	C 113.2 N 140.6 I
(2*S*,5*S*)-**3a**	94.5	−111.40 (*c* = 0.993)	2.0068	1.34	0.37[f], 0.38[g]	−0.01,[f] −0.40[g]	C 93.2 N* 143.8 I
(±)-**3b**	–	–	2.0070	1.33	0.38,[f] 0.38[g]	−0.21,[f] −0.28[g]	C 67.1 N 103.4 I
(2*S*,5*S*)-**3b**	94.9	−95.59 (*c* = 0.995)	2.0069	1.34	0.38,[f] 0.38[g]	−0.07,[f] −0.31 [g]	C 67.6 N* 101.7 I
(±)-**3c**	–	–	2.0073	1.37	0.36,[f] 0.37[g]	+0.38,[f] −0.40[g]	C 63.3 N 103.1 I
(2*S*,5*S*)-**3c**	96.9	−88.80 (*c* = 0.998)	2.0070	1.34	0.37,[f] 0.37[g]	−0.01,[f] −0.26[g]	C 79.3 N* 103.5 I
(±)-**3d**	–	–	2.0069	1.34	0.38,[f] 0.38[g]	+0.31,[f] −0.34[g]	C 71.5 N 103.1I
(2*S*,5*S*)-**3d**	95.8	−87.24 (*c* = 0.981)	2.0069	1.34	0.38,[f] 0.38[g]	−0.10,[f] −0.33[g]	C 71.2 N* 97.6 I

[a] Determined by HPLC analysis on a chiral stationary phase column (Daicel OD-H, 0.4 × 25 cm) and a mixture of hexane and 2-propanol (9:1) as the mobile phase. [b] Measured in THF. [c] Curie constant. [d] Weiss temperature. [e] Determined by DSC analysis upon heating. Standard notation gives the transition temperatures between the crystalline (C), liquid crystalline (N = nematic, N* = chiral nematic), and isotropic (I) states. [f] First heating process from the crystalline phase. [g] First cooling process from the isotropic phase.

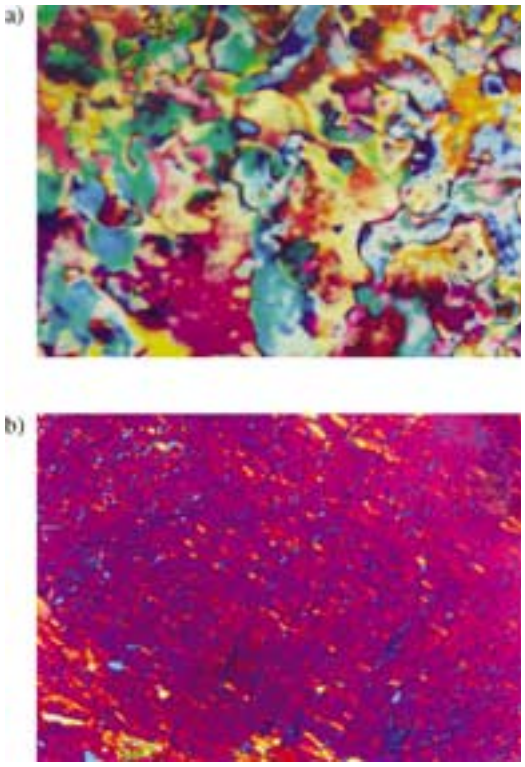

Figure 3. Optical polarized micrographs showing a) Schlieren texture of (±)-**3c** at 93.0 °C and b) oily streaks texture of (2*S*,5*S*)-**3c** at 83.0 °C.

showed weak ferromagnetic intermolecular interactions, whereas the other samples showed weak antiferromagnetic interactions. On the other hand, during the first cooling process from the isotropic phase, all of the samples except (±)-**3a** showed weak antiferromagnetic intermolecular interactions (Figure 4 and Table 1).[9] Noteworthy is the distinct change in the χ_{para} values observed at the crystal-to-LC phase transition during the first heating process; for example, (±)-**3c** showed an abrupt increase in χ_{para} at 342 K, followed by a sudden decrease at 378 K (Figure 4c). But during the cooling run from the isotropic phase, neither an appreciable decrease in χ_{para} nor the LC-to-crystal phase transition in the DSC curve were observed, owing to the considerable stability of the supercooled liquid-crystalline phase; the glassy phase was preserved for more than 24 h at 25 °C.

In contrast, for (2*S*,5*S*)-**3c** of 96.9 % *ee*, only a small increase in χ_{para} was noted upon the crystal-to-LC phase transition during the first heating process (Figure 4d). Such differences in the observed changes in χ_{para} values between the racemic and nonracemic samples can be accounted for by their molecular arrangement in the nematic and cholesteric phases, respectively; that is, the racemic nematic phase has only orientational order along the long molecular axis, whereas the nonracemic cholesteric phase has an additional helical superstructure with a twist axis perpendicular to the local director. The distinct increase in χ_{para} upon the phase change during the first heating process of (±)-**3c** is assumed to originate from the orientation of the molecules in the liquid-crystalline phase with the axis of maximum suscepti-

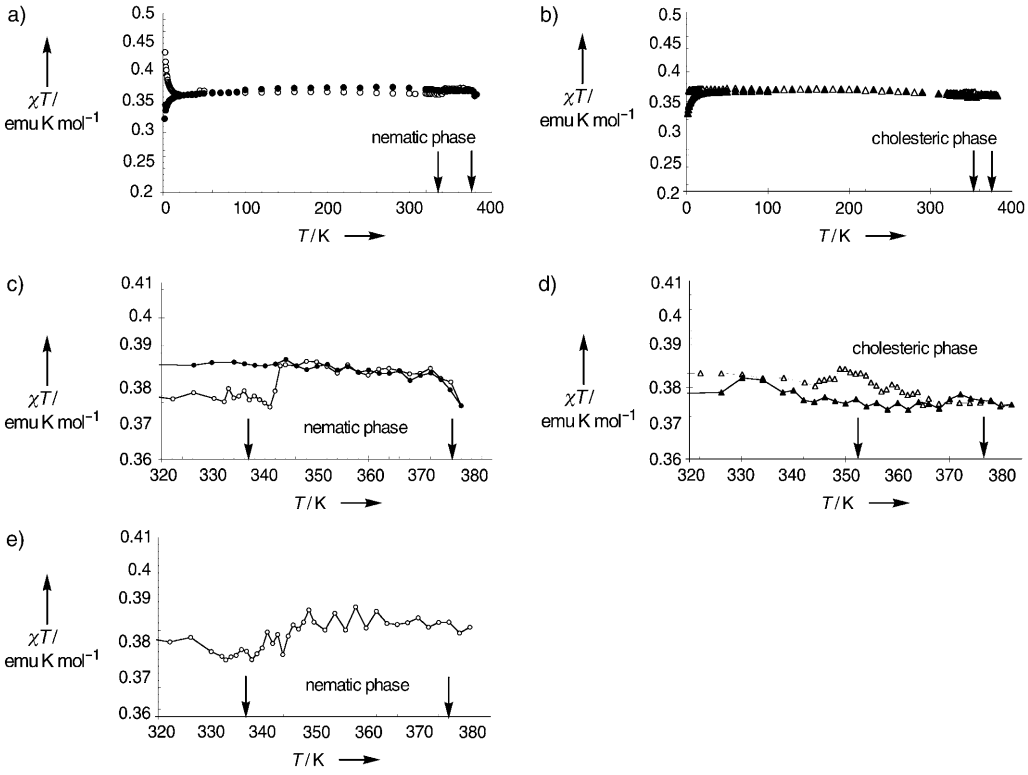

Figure 4. Temperature dependence of the magnetic susceptibility of a) (±)-**3c** and b) (2*S*,5*S*)-**3c** at the rate of 2 °C min^{-1} between 2 and 380 K at a field of 0.5 T, c) (±)-**3c** and d) (2*S*,5*S*)-**3c** at the rate of 0.5 °C min^{-1} between 320 and 380 K at a field of 0.5 T, and (e) (±)-**3c** at the rate of 0.5 °C min^{-1} between 320 and 380 K at a field of 0.05 T, measured during the first heating and cooling processes. ○ and △ represent the first heating process, ● and ▲ represent the first cooling process.

bility parallel to the magnetic field. Such an increase in χ_{para} upon the crystal-to-LC phase transition was also observed at a field of 0.05 T or below (Figure 4e). This is a rare example in which the orientation of the mesogens can be effected by very weak magnetic fields during the heating process.[1,2]

To gain better insight into the direction of the molecular orientation in the bulk LC in the magnetic field, the temperature dependence of the *g* value for **3c** was measured by EPR spectroscopy (Figures 5 and 6). During the heating process, the *g* value of (±)-**3c** gradually decreased in the crystalline state, then decreased abruptly upon the crystal-to-LC phase transition, and then became constant in the liquid-crystalline state. However, during the cooling process *g* was constant in the liquid-crystalline state and then gradually increased in the supercooled liquid-crystalline state (Figure 6a). As the *g* value of a nitroxyl group generally shows distinct anisotropy (in which the g_{xx} value along the NO axis is 2.008–2.009, the g_{zz} value along its $2p_z$ orbital axis is less than 2.003, and the g_{yy} value perpendicular to both axes is 2.005–2.006[10]), the observed decrease in *g* from 2.0065 to 2.0052 is assumed to correspond to the increasing contribution of the g_{yy} and g_{zz} values; that is, the majority of the molecules align in such a way that the NO axis is perpendicular to the applied magnetic field (Scheme 2). Accordingly, on the basis of the molecular structure of **3a** (Figure 2), the molecular long axis as well as the director axis should be approximately oriented parallel to the direction of the magnetic field. In contrast, for (2*S*,5*S*)-**3c**, *g* did not show any temperature dependence, and the value was almost constant between 2.0060 and 2.0070, close to the mean value in solution (Figure 6b); this result seems to reflect the peculiar helical superstructure of the cholesteric phase in which a uniform molecular orientation is impossible.[4]

Furthermore, a striking increase in the intensity of the EPR signal was observed for both racemic and nonracemic

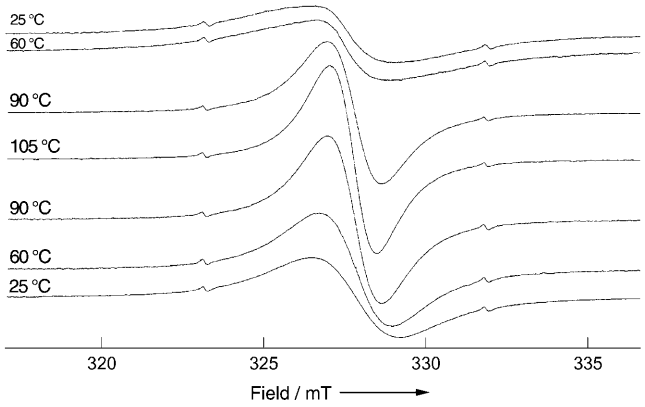

Figure 5. Selected EPR spectra of (±)-**3c** measured at various temperatures from the crystalline phase (top) through the liquid-crystalline phase to the supercooled liquid-crystalline phase (bottom).

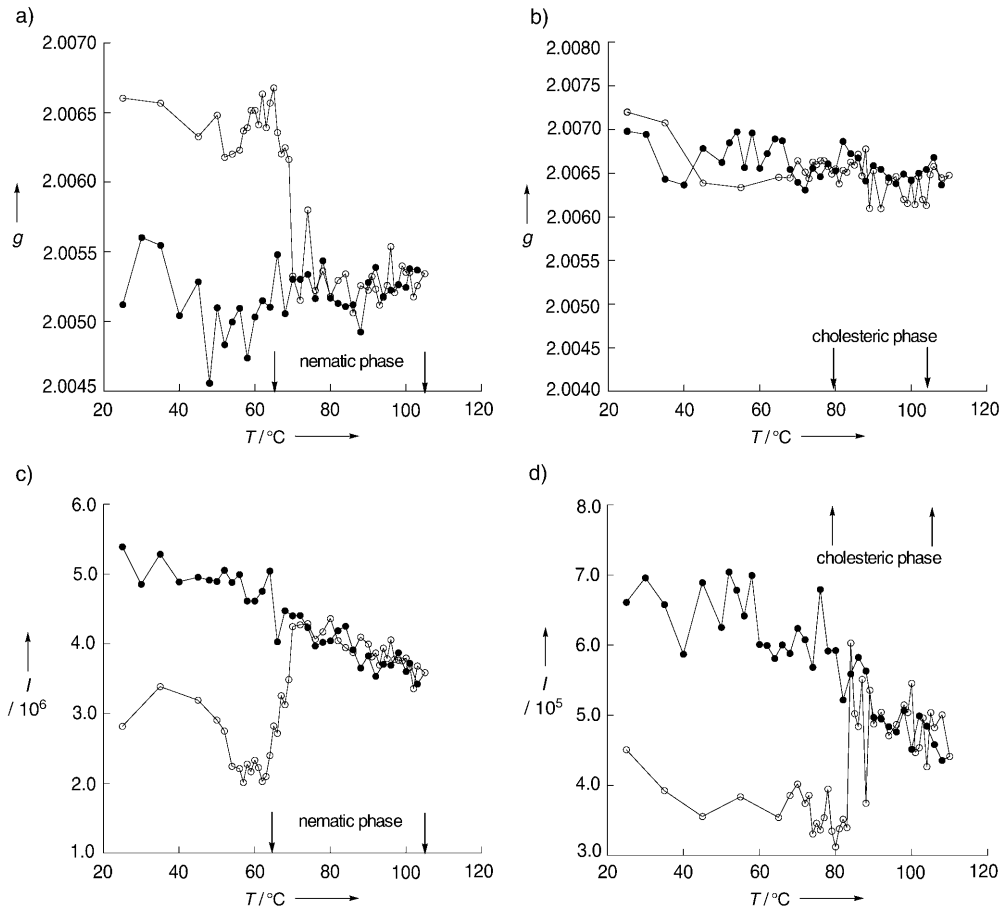

Figure 6. Variation of the *g* values of a) (±)-**3c** and b) (2*S*,5*S*)-**3c**, and the signal intensities of c) (±)-**3c** and d) (2*S*,5*S*)-**3c**, upon variation of the temperature; measured through the first heating (○) and cooling (●) processes.

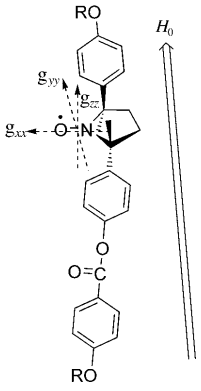

Scheme 2. Molecular orientation of **3** approximately parallel to the magnetic field (H_0).

samples of **3c** upon the phase transition observed during the heating process from the crystalline phase (Figures 6c and d). During the cooling process from the isotropic phase, the intensity gradually increased in the liquid-crystalline and the supercooled liquid-crystalline phases in both samples. In line with the intensity of the EPR signal being proportional to the χ value, a microscopic increase in the χ_{para} value was indeed observed upon the phase transition from the crystalline phase to the nematic or cholesteric phase.

We thus observed the microscopic decrease in the g value as well as the macro- and microscopic increases in the χ_{para} value upon the phase transition from the crystalline phase of (±)-**3c** to the liquid-crystalline phase during the heating process.

It is assumed that the molecular magnetic susceptibility anisotropy ($\Delta\chi$), which results from the cooperation of the paramagnetic and diamagnetic components originating from the nitroxyl group and the benzene rings, respectively, is responsible for the orientation of the bulk LC in the applied magnetic field. As $\chi_{\parallel}$ (parallel) is surely larger than $\chi_{\perp}$ (perpendicular) for (±)-**3c**, the experimental magnetic susceptibility anisotropy $\Delta\chi_{exp}$ was determined to be $+0.47\times10^{-4}$ emu mol^{-1} according to Equation (1),[2a] in which the

$$\Delta\chi_{exp}=\frac{3}{2}(\chi_{ordered}-\chi_{isotropic}) \quad (1)$$

experimental values of $\chi_{ordered}=+1.136\times10^{-3}$ emu mol^{-1} at 340 K (cooling process) and $\chi_{isotropic}=+1.105\times10^{-3}$ emu mol^{-1} at 340 K (heating process) were used.

Thus, it has been shown that a chiral racemic nematic phase is more suitable than a cholesteric phase with respect to the orientation of the bulk LC by weak magnetic fields. Alternatively, these paramagnetic LC substances may serve as dopants to align diamagnetic mesophases by weak magnetic fields, or as a real LC probe to investigate the dynamic behavior of a given diamagnetic LC material by EPR spectroscopy. Furthermore, if a paramagnetic chiral smectic (SmC*) phase is available, the orientation of the ferroelectric sample may also be controlled by application of weak magnetic fields.[11]

Received: March 16, 2004 [Z460007]

Keywords: chirality · EPR spectroscopy · liquid crystals · magnetic properties · phase transitions

[1] a) K. Griesar, W. Haase in *Magnetic Properties of Organic Molecules* (Ed.: P. M. Lahti), Marcel Dekker, New York, **1999**, pp. 325–344; b) P. Kaszynski in *Magnetic Properties of Organic Molecules* (Ed.: P. M. Lahti), Marcel Dekker, New York, **1999**, pp. 305–324; c) M. Marcos, J.-L Serrano, *Adv. Mater.* **1991**, *3*, 256–257.

[2] H. Müller, W. Haase, *J. Phys. (Paris)* **1983**, *44*, 1209–1213.

[3] a) K. Binnemans, Y. G. Galyametdinov, R. V. Deun, D. W. Bruce, S. R. Collinson, A. P. Polishchuk, I. Bikchantaev, W. Haase, A. V. Prosvirin, L. Tinchurina, I. Litvinov, A. Gubajdullin, A. Rakhmatullin, K. Uytterhoeven, L. V. Meervelt, *J. Am. Chem. Soc.* **2000**, *122*, 4335–4344; b) Y. Galyametdinov, M. A. Athanassopoulou, K. Griesar, O. Kharitonova, E. A. S. Bustamante, L. Tinchurina, I. Ovchinnikov, W. Haase, *Chem. Mater.* **1996**, *8*, 922–926; c) K. Griesar, Y. Galyametdinov, M. Athanassopoulou, I. Ovchinnikov, W. Haase, *Adv. Mater.* **1994**, *6*, 381–384.

[4] a) I. Dierking, *Texture of Liquid Crystals, Wiley-VCH, Weinheim*, **003**; b) S. T. Lagerwall, *Ferroelectric and Antiferroelectric Liquid Crystals, Wiley-VCH, Weinheim*, **999**; c) D. Demus, J. W. Goodby, G. W. Gray, H. W. Spiess, V. Vill, *Handbook of Liquid Crystals*, *Vol. 1–4*, Wiley-VCH, Weinheim, **1998**.

[5] a) S. Nakatsuji, M. Mizumoto, H. Ikemoto, H. Akutsu, J. Yamada, *Eur. J. Org. Chem.* **2002**, 1912–1918; b) J. Allgaier, H. Finkelmann, *Macromol. Chem. Phys.* **1994**, *195*, 1017–1030; c) M. Dvolaitzky, J. Billard, F. Poldy, *Tetrahedron* **1976**, *32*, 1835–1838; d) M. Dvolaitzky, J. Billard, F. Poldy, *C. R. Hebd. Seances Acad. Sci. Ser. C* **1974**, *279*, 533–535.

[6] a) S. Shimono, R. Tamura, N. Ikuma, T. Takimoto, N. Kawame, O. Tamada, N. Sakai, H. Matsuura, J. Yamauchi, *J. Org. Chem.* **2004**, *69*, 475–481; b) R. Tamura, S. Shimono, K. Fujita, K. Hirao, *Heterocycles* **2001**, *54*, 217–224; c) R. Tamura, S. Susuki, N. Azuma, A. Matsumoto, F. Toda, T. Takui, D. Shiomi, K. Itoh, *Mol. Cryst. Liq. Cryst.* **1995**, *271*, 91–96; d) R. Tamura, S. Susuki, N. Azuma, A. Matsumoto, F. Toda, Y. Ishii, *J. Org. Chem.* **1995**, *60*, 6820–6825; e) R. Tamura, S. Susuki, N. Azuma, A. Matsumoto, F. Toda, A. Kamimura, K. Hori, *Angew. Chem.* **1994**, *106*, 914–915; *Angew. Chem. Int. Ed. Engl.* **1994**, *33*, 878–880.

[7] a) N. Ikuma, R. Tamura, S. Shimono, N. Kawame, O. Tamada, N. Sakai, J. Yamauchi, Y. Yamamoto, *Mendeleev Commun.* **2003**, 109–111; b) J. Einhorn, C. Einhorn, F. Ratajczak, I. Gautier-Luneau, J.-L. Pierre, *J. Org. Chem.* **1997**, *62*, 9385–9388; c) N. Benfaremo, M. Steenbock, M. Klapper, K. Müllen, V. Enkelmann, K. Cabrera, *Liebigs Ann.* **1996**, 1413–1415; d) J. F. W. Keana, S. E. Seyedrezai, G. Gaughan, *J. Org. Chem.* **1983**, *48*, 2644–2647.

[8] The X-ray crystallographic data were collected at 298 K on an Enraf-Nonius Kappa CCD diffractometer. The crystal structure was solved by direct methods and refined by full-matrix least squares. All non-hydrogen atoms were refined anisotropically. All of the crystallographic calculations were performed by using the maXus software package.[12] Crystal data for (±)-**2a**: $C_{26}H_{36}NO_3$, $M_r=410.578$, $0.26\times0.20\times0.16$ mm^3, monoclinic, space group $C2/c$, $a=14.363(2)$, $b=15.1763(13)$, $c=22.269(4)$ Å, $\beta=99.155(7)°$, $V=4792.5(12)$ Å^3, $Z=8$, $\rho_{calcd}=1.138$ g cm^{-3}, $2\theta_{max}=50.72°$, $Mo_{K\alpha}$ ($\lambda=0.71073$ Å), $\mu=0.73$ cm^{-1}, ϕ-ω-scans, $T=298$ K, 4403 independent reflections, 2133 observed reflections ($I>2.0\sigma(I)$), 295 refined parameters, $R=0.064$, $R_w=0.166$, $\Delta\rho_{max}=0.320$ e Å^{-3}, $\Delta\rho_{min}=-0.341$ e Å^{-3}. Crystal data for (2*S*,5*S*)-**2a**: $C_{26}H_{36}NO_3$, $M_r=410.578$, $0.31\times0.21\times0.09$ mm^3, triclinic, space group $P\bar{1}$, $a=6.3786(2)$, $b=7.5419(3)$, $c=13.7089(9)$ Å, $\alpha=98.448(2)°$, $\beta=90.959(2)°$, $\gamma=114.567(4)°$, $V=591.06(5)$ Å^3, $Z=1$, $\rho_{calcd}=1.154$ gcm^{-3}, $2\theta_{max}=54.96°$, $Mo_{K\alpha}$($\lambda=0.71073$ Å), $\mu=0.74$ cm^{-1}, ϕ-ω-scans, $T=298$ K, 2611 independent reflections, 1396 observed reflections ($I>2.0\sigma(I)$), 277 refined parameters, $R=0.058$, $R_w=0.119$, $\Delta\rho_{max}=0.215$ e Å^{-3}, $\Delta\rho_{min}=-0.258$ e Å^{-3}. Crystal data for (2*S*,5*S*)-**3a**: $C_{33}H_{40}NO_5$, $M_r=530.685$, $0.36\times0.30\times0.03$ mm^3, monoclinic, space group $P2_1$, $a=7.1625(7)$, $b=9.696(2)$, $c=21.609(2)$ Å, $\beta=98.171(6)°$, $V=1485.5(4)$ Å^3, $Z=2$, $\rho_{calcd}=1.186$ g cm^{-3}, $2\theta_{max}=49.80°$, $Mo_{K\alpha}$($\lambda=0.71073$ Å), $\mu=0.79$ cm^{-1}, ϕ-ω-scans, $T=298$ K, 2733 independent reflections, 1809 observed reflections ($I>2.0\sigma(I)$), 424 refined parameters,

$R = 0.048$, $R_w = 0.091$, $\Delta\rho_{max} = 0.191$ e Å^{-3}, $\Delta\rho_{min} = -0.201$ e Å^{-3}. CCDC-233749–233751 contain the supplementary crystallographic data for this paper. These data can be obtained free of charge via www.ccdc.cam.ac.uk/conts/retrieving.html (or from the Cambridge Crystallographic Data Centre, 12, Union Road, Cambridge CB21EZ, UK; fax: (+44) 1223-336-033; or deposit@ccdc.cam.ac.uk).

[9] For recent reviews, see: a) *Magnetism: Molecules to Materials II* (Ed.: J. S. Miller, M. Drillon), Wiley-VCH, Weinheim, **2001**; b) S. Nakatsuji, H. Anzai, *J. Mater. Chem.* **1997**, *7*, 2161–2174 c) J. Veciana, J. Cirujeda, C. Rovira, J. Vidal-Gancedo, *Adv. Mater.* **1995**, *7*, 221–225. Also see ref [1].

[10] a) O. Takizawa, J. Yamauchi, H. O. Nishiguchi, Y. Deguchi, *Bull. Chem. Soc. Jpn.* **1973**, *46*, 1991–1995; b) O. H. Griffith, D. W. Cornell, H. M. McConnell, *J. Chem. Phys.* **1965**, *43*, 2909–2910.

[11] T. Kimura, T. Goto, H. Shintani, K. Ishizaka, T. Arima, Y. Tokura, *Nature* **2003**, *426*, 55–58.

[12] S. Mackay, C. J. Gilmore, C. Edwards, M. Tremayne, N. Stuart, K. Shankland, *maXus: A Computer Program for the Solution and Refinement of Crystal Structures from Diffraction Data*, University of Glasgow, Scotland, UK, Nonius BV, Delft, The Netherlands and MacScience Co. Ltd., Yokohama, Japan, **1998**.

[13] The Supporting Information contains Figure S1, in which the DSC curves and temperature-variable XRD patterns of (±)-**3c** and (2*S*,5*S*)-**3c** are shown.

